Desalination 491 (2020) 114534

Contents lists available at ScienceDirect

Desalination

journal homepage: www.elsevier.com/locate/desal

The techno-economic case for coupling advanced spacers to high-permeance RO membranes for desalination

K.Y. Toh[a], Y.Y. Liang[a,b,*], W.J. Lau[c], G.A. Fimbres Weihs[d,e]

[a] Faculty of Chemical and Process Engineering Technology, College of Engineering Technology, Universiti Malaysia Pahang, Lebuhraya Tun Razak, 26300 Gambang, Kuantan, Pahang, Malaysia
[b] Centre of Excellence for Advanced Research in Fluid Flow (CARIFF), Universiti Malaysia Pahang, Lebuhraya Tun Razak, 26300 Gambang, Kuantan, Pahang, Malaysia
[c] Advanced Membrane Technology Research Center, School of Chemical and Energy Engineering, Universiti Teknologi Malaysia, 81310 Skudai, Johor, Malaysia
[d] CONACyT–Instituto Tecnológico de Sonora, Departamento de Ciencias del Agua y Medio Ambiente, Cd. Obregón, Sonora 85000, Mexico
[e] The University of Sydney, School of Chemical and Biomolecular Engineering, NSW 2006, Australia

ARTICLE INFO

Keywords:
Spiral wound module
Advanced spacer
Permeance
Economic analysis
Operating conditions

ABSTRACT

Innovations in advanced materials in recent years have produced great improvements in the permeance of reverse osmosis (RO) membranes for desalination. This work presents a simplified techno-economic analysis for a representative advanced spacer and a high-permeance RO membrane under typical feed and operating conditions. The results agree with common trends for specific energy consumption (SEC). For high-permeance membranes, advanced spacers are more effective than conventional spacers in improving flux in the region close to the inlet, due to a fast decrease in Reynolds number along the channel. The total cost for seawater RO (SWRO) and brackish water RO (BWRO) could be reduced by 7.5% and 32%, respectively by increasing the membrane permeance to 10 L/m^2.h.bar regardless of the spacer type used. However, as feed velocity has negligible effects on total cost for high-permeance membrane systems, further cost reductions with larger membrane permeances are limited due to significant concentration polarisation and lower mass transfer. Nevertheless, when operating SWRO at constant recovery, those levels of cost reduction can be achieved with an advanced spacer at half of that membrane permeance value. This highlights that more cost-effectiveness can be gained by improving the spacer efficacy than by increasing membrane permeance.

1. Introduction

Reverse osmosis (RO) membrane technology is the most popular water purification method for desalination processes nowadays. Because of the high energy and pressure requirements for the desalination of seawater (> 6 MPa) and brackish water (> 1 MPa), the energy consumption for RO represents the largest portion of the total water cost [1,2]. Thus, one of the main current research priorities for RO processes is to reduce their energy consumption to make them more sustainable and economically viable in the future [3].

Some approaches to reduce the energy consumption and environmental impact of membrane-based desalination processes are: 1) employing high-permeance membranes to obtain larger permeate flows at the same operating pressure [4–6]; 2) employing high-efficiency energy recovery devices (ERD) to recover energy from the retentate [7–9]; 3) improving membrane module design and/or optimising operating conditions [10,11]; and 4) utilizing advanced pre-treatment processes with minimum usage of chemicals for RO feed water to reduce membrane fouling in spiral wound membrane (SWM) modules [9,12,13]. Of these approaches, improving the water permeability of the membrane is given the most attention, mainly because it is the “heart” of the entire desalination process. However, at current membrane permeance levels, further improvements have shown an asymptotic curve in terms of the reduction in energy requirements due to thermodynamic and mass transfer limits. Nevertheless, further gains in terms of capital cost savings are achievable with the use of fewer pressure vessels when high-permeance membranes are employed [4].

Typically, commercial RO membranes with high sodium chloride (NaCl) rejection (at least 99.7%) only exhibit permeance values of 1–3 L m^{-2} h^{-1} bar^{-1} [14–16]. Over the past 10–20 years, there has been very little progress in terms of utilizing new materials for manufacturing commercial thin film composite (TFC) RO membranes. The main method for producing the selective layer (i.e., polyamide) of commercial TFC RO membranes is via the interfacial polymerisation

* Corresponding author at: Faculty of Chemical and Process Engineering Technology, College of Engineering Technology, Universiti Malaysia Pahang, Lebuhraya Tun Razak, 26300, Gambang, Kuantan, Pahang, Malaysia.
E-mail address: yongyeow.liang@ump.edu.my (Y.Y. Liang).

https://doi.org/10.1016/j.desal.2020.114534
Received 10 January 2020; Received in revised form 8 May 2020; Accepted 12 May 2020

reaction between trimesoyl chloride (TMC) and *m*-phenylene diamine (MPD) [17,18]. To the best of our knowledge, only two new generations of TFC membranes currently available in the market are manufactured using advanced materials. They are the thin film nanocomposite (TFN) RO membranes (NanoH_2O™) developed by LG Chem by incorporating inorganic nanofillers into polyamide layer [19,20] and the membrane manufactured by Aquaporin Inside® by embedding aquaporin proteins into the selective layer [21]. These membranes demonstrate better flux and rejection compared to the conventional TFC membrane due to improvements in the polyamide layer such as higher hydrophilicity and the presence of special water channels [20,21].

Recently, Shi et al. [22] highlighted that high-permeance RO membranes with permeance in the range of 3–7 L m^{-2} h^{-1} bar^{-1} could be achieved when testing with 2000 ppm NaCl saline solution. Such high-permeances are obtained by approaches such as synthesising the selective layer using high-flux natural materials, modifying the polyamide layer by incorporating hydrophilic nanomaterials and modifying the microporous substrate of TFC membranes. Given the remarkable progress in the 2D structure and tuneable physicochemical properties of graphene oxide (GO), it is very likely that ultrathin freestanding GO membrane films with ultra-high-permeance values in the range of 8–27.6 L m^{-2} h^{-1} bar^{-1} could be fabricated [23,24]. Nevertheless, it must be pointed out that such freestanding GO membranes, which are still in the early stage of development, have a relatively low rejection against monovalent salts (i.e., < 50%).

With respect to energy requirements, Cohen-Tanugi et al. [4] found that a significant increase in membrane permeance (3 times higher than the control conditions) could decrease the number of pressure vessels and energy consumption by 44% and 15% respectively, for seawater reverse osmosis (SWRO) plants when compared with current membranes at the same capacity and recovery rate. For brackish water reverse osmosis (BWRO) plants, a greater reduction in the number of pressure vessels (by 63%) and energy usage (by 46%) could be achieved when membrane permeance was tripled. However, further increases in energy savings are less likely for the case where an even higher permeance membrane is used (3–4.5 L m^{-2} h^{-1} bar^{-1}), mainly because of the higher concentration polarisation (CP) at the membrane surfaces.

In order to increase membrane water flux, efficient mixing is required to minimise CP [25–28]. Despite this, there have been no studies to date focusing on the effect of advanced spacers on CP for high-permeance membranes. The benefits of using advanced spacers instead of conventional spacers include improved permeation flux [29–31], reduced pressure loss [29,31–33] and a reduced tendency for membrane fouling [29,31,32]. Although an increase in mass transfer is typically accomplished at the expense of higher pressure drop, Guillen and Hoek [34] in their 2D computational fluid dynamics (CFD) study of advanced spacer geometries noted that pressure loss due to an improved spacer geometry may not substantially reduce module performance for RO, especially for high salinity water desalination systems. This is because typical pressure losses in SWM modules (~0.05 MPa) are very small compared to the typical inlet operating pressure (~6 MPa).

Since the permeate flux in SWM is not only controlled by the driving force, but also by the degree of mixing or CP phenomenon caused by the advanced spacer, the extent to which an advanced spacer geometry would be more beneficial than their conventional spacer counterpart (i.e., 2-layer non-woven) for SWRO and BWRO is unclear. Although recent developments in proposed advanced/novel spacer geometries have shown significant improvement in terms of permeate flux, the tests for those new spacers have only been conducted either in small-scale CFD studies [30,35] or lab-scale experiments [31,36–38]. Hence, the relative benefit of advanced spacers on flux enhancement for a large-scale module in comparison with conventional spacer designs remains unclear. This study analyses the effect of implementing a hypothetical advanced spacer with higher mass transfer and lower pressure loss features in a full-scale membrane module, in order to compare its performance against a conventional spacer design. This study can therefore shed insights into whether future research directions should focus more on improving spacers or membrane permeance.

It is also worth noting that the performance of RO systems is sensitive to different operating and feed conditions [10]. However, there is no clear understanding of the effects of operating and feed conditions on cost-effectiveness, especially for high-permeance membranes. Thus, our work also investigates the effects of advanced spacers as well as operating and feed conditions on permeate flux, mass transfer coefficient, CP index and on overall system performance (in terms of total water processing cost), in combination with high membrane permeance for both SWRO and BWRO.

A reliable model-based analysis is useful for designing and improving RO systems. In our recent work [39], we developed a multi-scale approach in which detailed results obtained for mass transfer and pressure drop from small-scale (i.e., sub-millimetre) CFD simulations are used to predict the overall performance for an actual size of SWM (i.e., a few metres in length). This mechanistic model thus captures important operating factors that interplay between the permeate flux, CP, recovery rate and pressure drop of an entire SWM module. Our previous study [39] also showed that the mass transfer coefficient alone is insufficient to evaluate the efficiency of a spacer for RO systems.

There are several tools for evaluating membrane performance such as specific energy consumption (SEC) [40–42], specific power consumption (SPC) [25,26,43,44], spacer configuration efficacy (SCE) [25,26,44], spacer performance ratio (SPMP) [26,45] and economic analysis [46]. Of those, an economic analysis is a more appropriate tool because it can be used to evaluate the economic impacts of energy consumption, rather than inferring them from proxy indicators. However, an accurate economic analysis is very tedious [47,48]. Despite this, it is possible to carry out an insightful membrane module efficiency comparison by using a simplified economic analysis, as developed in our previous work [39], that takes into account the most important relevant parameters, i.e., pre-treatment costs, operating pressure, pressure drop and capital costs. Hence, this work aims to use a simplified economic model to identify the most important factors driving the minimisation of the total water processing cost when using advanced spacers and high-permeance membranes under different operating conditions.

2. Methodology

2.1. Multi-scale modelling

A multi-scale modelling approach solves multiple models at different scales (sizes or reference lengths) simultaneously to describe a system. In this work, correlations for the dependence of Sherwood number (dimensionless measure for mass transfer) and Fanning friction factor (dimensionless measure for pressure loss) on Reynolds number are taken from a small scale model (sub-millimetre) solved using CFD [39]. These correlations are used to solve a large-scale model of the full-sized SWM module (i.e., a few metres in length) in order to predict the overall membrane module performance with respect to permeate flux and pressure drop.

Despite the numerous spacer optimisation studies in the literature, it is difficult to increase mass transfer and reduce pressure drop simultaneously. However, some researchers [31,49] argue that certain spacer geometries have promising results in terms of flux enhancement and pressure drop reduction. For instance, an optimal multi-layer structure (i.e., twisted spacer as middle spacer and non-woven net as outer layer) shows a Sherwood number approximately 30% higher than an optimal non-woven spacer at the same energy consumption, and only about 40% of the energy consumption of the optimal non-woven spacer at the same Sherwood number [49]. Another recent study is the 3D advanced spacer based on triply periodic minimal surfaces (TPMS) proposed by Sreedhar et al. [31] who found a 15.5% flux improvement for BWRO and up to 12.5% pressure drop reduction when compared to

Table 1
Correlations for the dependence of Sh and f_{glob} on Re_h for the conventional and advanced spacer configurations.

Spacer	Correlations	
Conventional spacer (2LNW) [39]	$Sh = 2.44Re_h^{0.61}$	$f_{glob} = 8.76Re_h^{-0.62}$
Advanced spacer	$Sh = 3.66Re_h^{0.61}$	$f_{glob} = 4.38Re_h^{-0.62}$

a conventional spacer geometry. Thus, this paper explores the best-case scenario, and examines possible consequence of such development, by comparing the performance of a hypothetical advanced spacer that can consistently achieve a 50% higher Sherwood number (Sh) and a 50% lower Fanning friction factor (f_{glob}) than the conventional 2-layer non-woven spacer simulated in our previous work [39].

The dependencies of Sh and f_{glob} on Reynolds number for the conventional spacer have been previously validated elsewhere [39] and are now shown in Table 1. Those correlations are multiplied by factors of 1.5 and 0.5, respectively to yield the correlations for Sh and f_{glob} of the hypothetical advanced spacer as shown in Table 1.

It is important to note that the correlations for the conventional spacer (2LNW) were developed under the condition of impermeable wall [39]. Nevertheless, it is possible to convert the data for an impermeable dissolving wall to a permeable membrane case under conditions where the ratio (ψ) of volumetric flux to impermeable mass transfer coefficient is below 20 [50]. Given that the values of ψ for all permeances considered in this paper are below 2, it is safe to assume that this correlation is valid for calculating the permeable wall mass transfer coefficient, for the conditions simulated in this paper.

The large-scale model solves a system of coupled 1D ordinary differential equations (ODEs) for the global and salt mass balances, as well as an ODE for pressure drop along the membrane module length:

$$\frac{dQ}{dx} = -\frac{A_m J}{\rho L} \tag{1}$$

$$\frac{dw_b}{dx} = \frac{A_m J}{\rho Q L}(w_b - w_p) \tag{2}$$

$$\frac{dp}{dx} = \frac{2\rho u_{eff}^2}{d_h} f_{glob} \tag{3}$$

The 1D ODE model in Eqs. (1) to (3) is derived from first principles (viz. mass and momentum balances). These equations can be solved using a Runge-Kutta type method but require inputs such as permeate flux (J) and f_{glob}. In order to obtain these inputs for the different points along the SWM module, the k_{mt} and f_{glob} values are calculated from the correlations in Table 1, and then used to calculate the local flux values in the axial direction [4,22,51–54]. The details of the flux calculation methodology have been previously reported [39,55], and can be found in Appendix A. Finally, the total volumetric flow rate for the permeate (Q_p) is calculated by integrating the flux along the module:

$$Q_p = \delta_{ch} \int_0^L \frac{J}{\rho} dx \tag{4}$$

For simplicity, the flow is assumed to be isothermal and only the feed side is modelled, rather than both feed and permeate channel. This is because the permeate pressure is relatively small (i.e., 0.1 to 1 bar) compared to the inlet transmembrane pressure ($\Delta p_{tm,in}$) (i.e., of the order of 10 bar). This simplification is further supported by the economic analysis in our previous work [39], which reported that changes in pressure losses along the channel have a marginal effect on the total processing cost [39]. In addition, Karabelas et al. [42] found that the friction losses in the permeate channel only contributed about 0.1–0.4% of the total SEC. In terms of mass transfer, Avlonitis et al. [56] found good agreement between their one-dimensional mass transfer model prediction and data obtained from operating RO seawater desalination plant. Thus, the assumption of 1D ODEs, that is, Eqs. (1), (2) and (3), is justifiable given that the pressure drop and mass transfer vary mostly in the feed flow direction [4]. The results of the large-scale model are used to predict the total permeate flow rate and pressure drop, which are then used in the economic part of the model.

Table 2
Parameters for the cases modelled in this paper.

Parameter	Value for SW	Value for BW
Feed velocity, u_{avg} (m/s)	0.07–0.135	
Intrinsic rejection, R_{int} (%)	99.6	97
Membrane permeance, L_p (L m^{-2} h^{-1} bar^{-1})	1–10	3–10
Feed mass fraction, $w_{b,in}$	0.035–0.041	0.002–0.0035
Inlet transmembrane pressure, $\Delta p_{tm,in}$ (MPa)	6.5–8	1.5–2

The parameters used for the cases that are simulated using the large-scale model are tabulated in Table 2. In order to evaluate the cost-effectiveness of high permeance membranes, permeance ranges between 1 and 10 L m^{-2} h^{-1} bar^{-1} for seawater (SW), and between 3 and 10 L m^{-2} h^{-1} bar^{-1} for brackish water (BW) are considered. The choice of these ranges is justifiable following the remarkable progress in advanced materials for constructing membranes with high-permeance properties [23,24]. The effect of membrane permeance on membrane performance is further discussed in Section 3.1.

Since the $\Delta p_{tm,in}$ and feed flow conditions have notable effects on mass transfer and concentration polarisation [5], the conditions for optimising high permeance membrane performance may be different compared to the case using typical permeance membranes. Addressing these research questions is important in order to improve module design and develop membranes/spacers with better anti-fouling properties for desalination processes. In this work, $\Delta p_{tm,in}$ values in the range of 6.5–8 MPa and 1.5–2 MPa are used for SW and BW desalination, respectively. A lower $\Delta p_{tm,in}$ is used for BW desalination due to lower osmotic pressure of the feed solution in comparison to SW.

With respect to feed velocities, values between 0.07 and 0.135 m/s are considered for both SW and BW desalination. This range is within the flow velocities used in practice (0.07–0.2 m/s [57]) for a typical channel height (≈1 mm). In addition, the highest value of flow velocity considered (i.e., u_{avg} = 0.135 m/s) is the value recommended by SWM manufacturers [58]. This value corresponds to a Reynolds number (Re_h) of about 200. The choice of feed water concentration for SW and BW shown in Table 2 is justifiable, given that seawater has an average total dissolved solid (TDS) of about 35,000 ppm, whereas brackish water has a concentration that is about one magnitude smaller than seawater [59]. The effects of $\Delta p_{tm,in}$ and feed conditions (i.e., inlet velocity and concentration) are respectively discussed in Sections 3.2 and 3.3.

Constant properties (i.e., viscosity and diffusivity) can be assumed for RO given that the flux and concentration polarisation for RO is much lower than for ultrafiltration (UF) [60]. The diffusivity value used corresponds to a Schmidt number of about 600, which is representative of NaCl, the most abundant solute usually encountered in RO systems [61,62], and which has been shown to be a good approximation for modelling the behaviour of seawater in desalination processes [63].

2.2. Theoretical background of techno-economic analysis

2.2.1. Techno-economic analysis in a typical RO desalination process

Fig. 1 shows a schematic representation of a typical single-stage RO desalination process with 4 membrane elements per vessel. The feed solution (seawater or brackish water) is first treated (typically via a coagulation/flocculation process followed by media filtration) to reduce its turbidity level before being delivered to the membrane desalination process. In the desalination process, the water is pressurised to pass through the RO membrane to produce water of high purity (i.e., permeate). The rejected solution with much higher solute concentration (i.e., brine) is then passed through an energy recovery device (ERD) in

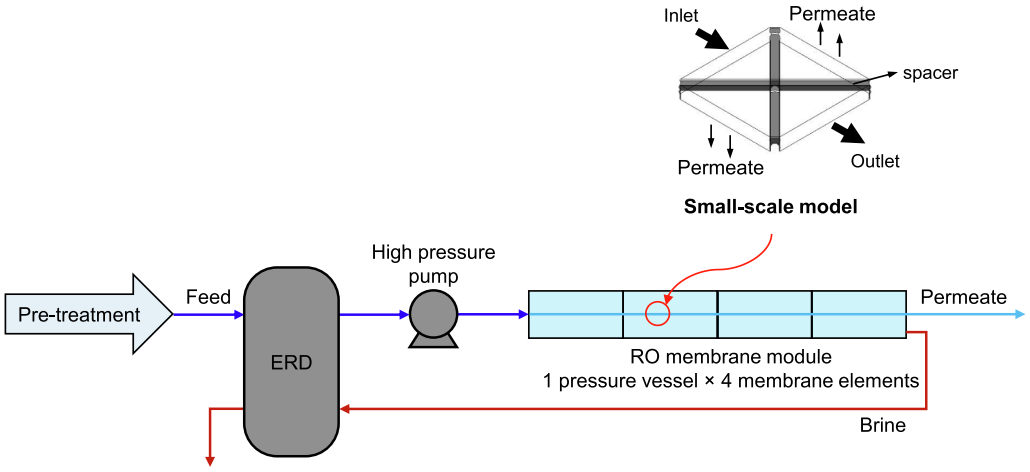

Fig. 1. Schematic representation of typical RO desalination process.

which some of solution pressure is recovered. It is worth noting that energy recovery is more significant in reducing the total processing cost for SWRO than for BWRO, due to the lower recovery rate of the former [39]. Therefore, ERD is typically only required for SWRO desalination plant. No post-treatment is shown in Fig. 1 because the cost associated with post-treatment is significantly lower than that of pre-treatment in a desalination process [64] and can thus be neglected. Overall, only three important processes, namely pre-treatment, pressurisation and membrane separation, are considered in this work for the simplified economic analysis of a typical RO desalination process.

Techno-economic analysis is a crucial tool to analyse the cost-effectiveness of modifications to a process, by estimating the product selling price through consideration of engineering-based process design, economic computations and financial assessment [65]. An ideal techno-economic analysis would require a series of detailed calculations of material and energy balances, unit operational capital and operating cost estimations. Hence, a complete economic analysis would consider the costs of the entire desalination plant as well as several other parameters (e.g., salaries and interest rate) to determine the total water production cost. However, carrying out a complete economic analysis is very complicated because it can be greatly affected by geographical and time factors including human resources, equipment costs and interest rates. Nevertheless, simplifications to a complex economic analysis can be used to compare cost trends. The analysis proposed in this paper considers several key parameters in quantifying water cost, namely pre-treatment, operating pressure, pressure drop and capital expenses, in order to gain valuable insights into the effect of using advanced spacer geometries and high-permeance membranes.

2.2.2. Techno-economic modelling

The costs of fouling and cleaning are usually proportional to the membrane area. Thus, these costs can be assumed to be included in the membrane cost [55]. Although TFN RO membranes manufactured by LG Chem [19] perform better than conventional TFC RO membranes, their market price is commercially competitive. In view of this, the costs for conventional and advanced RO membranes are assumed to be the same in this analysis. The cost of the spacer mesh is also assumed to be included in the membrane cost given that the spacer is an inexpensive part of the SWM [66]. As spacers are typically made of polypropylene [37,67], the mass production cost of regular and advanced spacer designs can be assumed to be similar. It should be noted that the simplified economic model used here only considers the changes in operational costs related to different spacers, i.e., conventional vs advanced spacer, and membrane permeance used by assuming all other costs such as pre-treatment, membrane capital and costs related to elevating the pressure to the operating condition remain constant. In this manner, this simple economic model can be used to compare different spacer designs in a like-for-like basis.

Although the details of this simplified techno-economic analysis have been previously reported [39], they are still important in this work for results interpretation. Thus, the information is summarised here for the benefit of the readers. The simplified total processing cost (c_{total}) can be expressed as follows.

$$c_{total} = \frac{F_a}{t_{op}} A_m c_m + c_{pt} Q_{in} + \frac{c_e}{\eta_{pump}} [Q_f (p_{in} - p_a) - \eta_R Q_r (p_r - p_a)] \quad (5)$$

where the right-hand side terms of the equation are the amortised membrane capital cost, the feed pre-treatment cost and the pumping energy cost. In particular, energy recovery is taken into account by subtracting the recovered energy, that is the product of the retentate flow rate (Q_r), the retentate gauge pressure ($p_r - p_a$) and the pressure recovery efficiency (η_R) from the pumping energy required at the feed ($Q_f \Delta p_{tm,in}$). Dividing Eq. (5) by the permeate flow rate (Q_p) and making use of the definitions for recovery rate ($R_r = Q_p/Q_f$), retentate flow rate ($Q_r = Q_f - Q_p$), inlet transmembrane pressure ($\Delta p_{tm,in} = p_{in} - p_a$) and channel pressure drop ($\Delta p_{ch} = p_{in} - p_r$), we obtain an equation for the total unit processing cost per unit permeate flow rate (C_{total}) as follows.

$$C_{total} = \frac{A_m c_m F_a}{Q_p t_{op}} + \frac{c_{pt}}{R_r} + \frac{c_e}{R_r \eta_{pump}} [\Delta p_{tm,in} - \eta_R (1 - R_r)(\Delta p_{tm,in} - \Delta p_{ch})] \quad (6)$$

where the first term on the right-hand side of Eq. (6) is the annualised capital cost of the membrane per unit of permeate (C_c), the second term is the pre-treatment cost per unit permeate (C_{pt}), and the last term is the energy cost per unit permeate. The last term can be further rearranged to identify the contributions to the energy cost due to the inlet operating pressure (C_{op}) and the pressure drop along the membrane module (C_{dp}):

$$C_{op} = \frac{c_e}{R_r \eta_{pump}} [1 - \eta_R (1 - R_r)] \Delta p_{tm,in} \quad (7)$$

$$C_{dp} = \frac{c_e}{R_r \eta_{pump}} \eta_R (1 - R_r) \Delta p_{ch} \quad (8)$$

The simplified total unit processing cost then becomes:

$$C_{total} = C_c + C_{pt} + C_{op} + C_{dp} \quad (9)$$

The parameters used for the techno-economic analysis are summarised in Table 3.

It shall be noted that the recovery rate obtained depends on the operating condition and intrinsic membrane permeance used. The range for recovery rate used in this study for SWRO and BWRO are

Table 3
Case study parameters used for the techno-economic analysis.

Parameter	Values
Membrane area of module (A_m)	28 m^2
Number of envelopes (N)	14
Module length (L)	1 m
Channel width per membrane sheet (δ_{ch})	1 m
Number of modules per pressure vessel	4 units
Channel height (h_{ch})	1 mm
Energy cost (c_e)	\$0.15/kWh
Membrane cost (c_m)	\$40/m^2
Amortisation factor (F_a)	0.15/yr
Pump efficiency (η_{pump}) [42]	0.85
Operation time (t_{op})	7500 h/yr
Retentate pressure recovery efficiency (η_R) [4,42]	0 for BW, 0.95 for SW
Pre-treatment cost per unit feed (c_{pt})	\$0.03/m^3

33–65% and 60–93%, respectively, which are similar to those reported in the literature, i.e., 35–50% and 50–85% for standard SWRO and BWRO, respectively [6].

2.3. Comparison between techno-economic analysis and specific energy consumption (SEC)

The available data for SEC in the literature [4,68] were used to compare with the results obtained from the techno-economic analysis in this work in order to establish confidence in the model prediction. This comparison is justified, given that the main component of the total processing cost (C_{total}) is the operating pressure cost, which contributes 70–90% of the simplified total cost. Two cases from the literature which were examined under similar operating conditions as our work (i.e., $w_{b,in} = 0.032$ with $\eta_{pump} = 0.85$ for SWRO [68] and $w_{b,in} = 0.002$ with $\eta_{pump} = 0.75$ for BWRO [4]) are selected for comparison purpose. The main findings reported in the literature in terms of SEC [4,68] can be used to validate the trends for the economic analysis presented in this work, as highlighted in Section 3.1.

3. Results and discussion

3.1. Effect of intrinsic membrane permeance

Fig. 2 shows the local permeate flux values along the membrane module for SWRO and BWRO, at the lower and upper limit of permeance, for conventional (CS) and advanced spacers (AS). For the region close to the inlet of the membrane module (i.e., $x < 0.6$ m for SWRO and $x < 2$ m for BWRO) for a high-permeance membrane, the advanced spacer shows the largest permeate flux because it yields the largest *Sh* and a lower pressure drop at a given Reynolds number (as predicted by the expressions in Table 1). However, the large flux also results in a quick reduction of the Reynolds number along the module, which leads to a reduction in mass transfer. The fast decrease in Reynolds number along the channel explains why the conventional spacer (2LNW) shows greater flux than the advanced spacer closer to the module outlet (i.e., $x > 0.6$ m for SWRO and $x > 2$ m for BWRO) for the high-permeance membranes. A similar trend is also observed for the low-permeance membranes, albeit at a larger membrane length (i.e., $x > 4$ m for SWRO and $x > 5$ m for BWRO, not shown in Fig. 2).

It is also important to note that the permeate flux for a high-permeance membrane approaches zero at a shorter module length (i.e., $x \approx 2$ m for SWRO and $x \approx 4$ m for BWRO) than for the low-permeance membrane. This means that a careful selection of module length for high-permeance membranes is paramount, because the membrane area is wasted in the downstream region where flux is near-zero. It has been reported that the SEC for BWRO remains unchanged when the number of membrane modules exceeds 4 units [69]. Thus, for simplicity of analysis, 4 modules (or an effective membrane length of 4 m in a single pressure vessel) is used for the techno-economic analysis for both BWRO and SWRO in the latter part of this study.

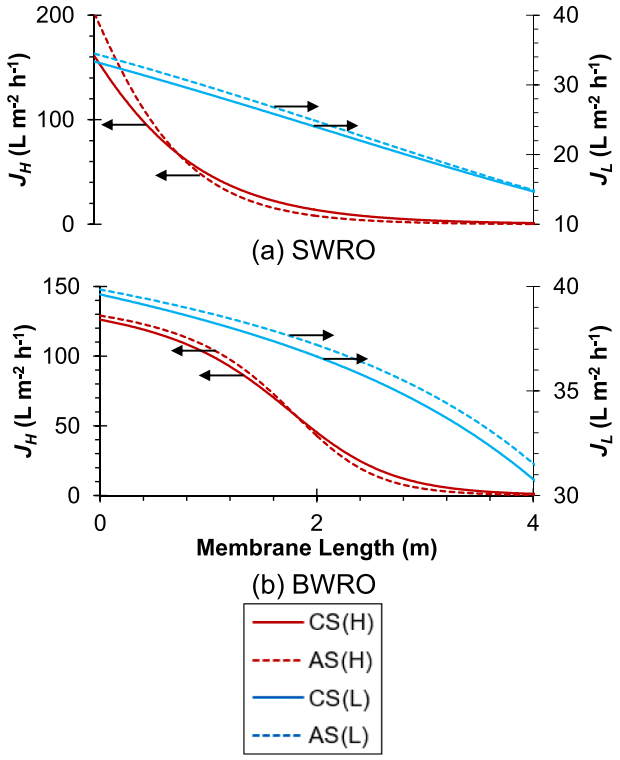

Fig. 2. Local permeate flux along membrane module for the conventional (CS) and advanced spacers (AS), for (a) SWRO and (b) BWRO at the same inlet TMP ($\Delta p_{tm,in,\ SW} = 6.5$ MPa and $\Delta p_{tm,in,\ BW} = 1.5$ MPa). 'L' and 'H' in the figure legend denote low ($L_{p,SW} = 1$ L m^{-2} h^{-1} bar^{-1} and $L_{p,BW} = 3$ L m^{-2} h^{-1} bar^{-1}) and high ($L_{p,SW} = L_{p,BW} = 10$ L m^{-2} h^{-1} bar^{-1}) intrinsic membrane permeance, respectively.

For a given membrane length (i.e., 4 m as indicated in Table 3), Fig. 3 shows the effect of the advanced spacer on total processing cost (C_{total}) and recovery rate (R_r) as the membrane permeance is varied. It can be observed that the advanced spacer considered reduces C_{total} by only 1–2% at a low-permeance for both SWRO and BWRO. At a larger membrane permeance, on the other hand, advanced spacer shows negligible changes in C_{total} and R_r compared to the conventional spacer for both SWRO and BWRO. This is because of the trade-off between local flux and mass transfer along the membrane channel, as shown in Fig. 2. However, the data suggest that an advanced spacer would result in a larger average flux if a shorter membrane length is used, and can therefore lower processing costs compared with the conventional spacer.

When the feed flow rate is substantially decreased along the membrane channel due to a larger permeate flux, a tapered-array configuration might be the best configuration for high-permeance membrane. In such an array, there would be more modules in parallel in the first section, followed by subsequent sections with less modules in parallel. Higher recovery is attainable because a tapered-array configuration allows a reduction in cross-sectional area over the series array configuration; hence, it is more suitable for systems with a significant reduction in cross-flow due to permeation [70]. The key challenge in optimising such a design is identifying the critical cross-flow velocity at which it is not economical or viable to increase the membrane module length. However, this could be achieved using the multi-scale modelling analysis presented in Section 2.1.

Fig. 3 also shows that the total processing cost for brackish water and seawater can be significantly reduced by 32% and 7.5%, respectively, when the L_p is increased to 10 L m^{-2} h^{-1} bar^{-1}. These results

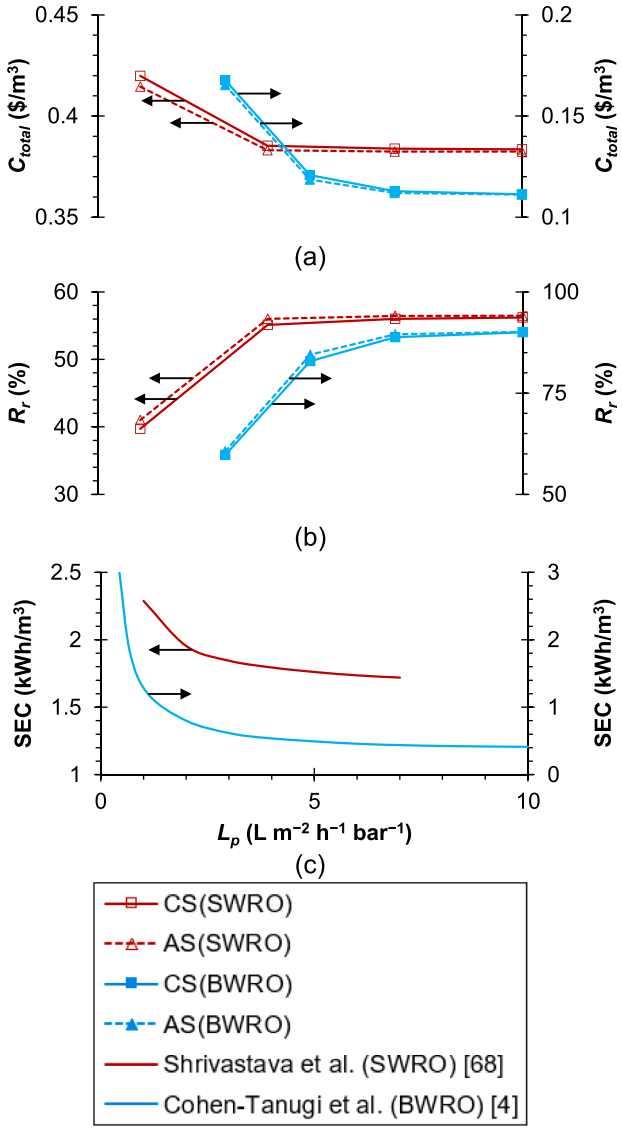

Fig. 3. Effect of intrinsic membrane permeance on (a) total processing cost (C_{total}), (b) recovery rate (R_r) and (c) specific energy consumption [4,68] at the same inlet TMP ($\Delta p_{tm,in,\ SW}$ = 6.5 MPa and $\Delta p_{tm,in,\ BW}$ = 1.5 MPa).

agree with the simulation findings reported in the work of Cohen-Tanugi et al. [4] in which the energy savings for brackish water (46%) are greater than that of seawater (15%) when L_p is tripled. This is because the recovery rate (or flux) for BWRO (61% to 90%) increases at a faster rate than for SWRO (40% to 56%). However, the total cost remains unchanged at a higher L_p ($>$ 4 L m^{-2} h^{-1} bar^{-1} for seawater and $>$ 7 L m^{-2} h^{-1} bar^{-1} for brackish water), suggesting there is no benefit in increasing L_p in the case where module length increases beyond 4 m. This trend is similar to findings reported by Shrivastava et al. [68] and Cohen-Tanugi et al. [4] (Fig. 3c) in which they found that energy savings are negligible when L_p exceeds 4 and 5 L m^{-2} h^{-1} bar^{-1} for seawater and brackish water, respectively. Thus, this provides confidence in the techno-economic model predictions presented in this paper.

The reason why the total processing cost remains similar at a higher L_p can be explained by a larger average CP and a lower average k_{mt} (Fig. 4) at a higher L_p, which limit further increases in R_r or flux as L_p increases. Moreover, the combined two factors (i.e., larger CP and lower k_{mt}) could lead to a larger tendency of scaling/fouling and

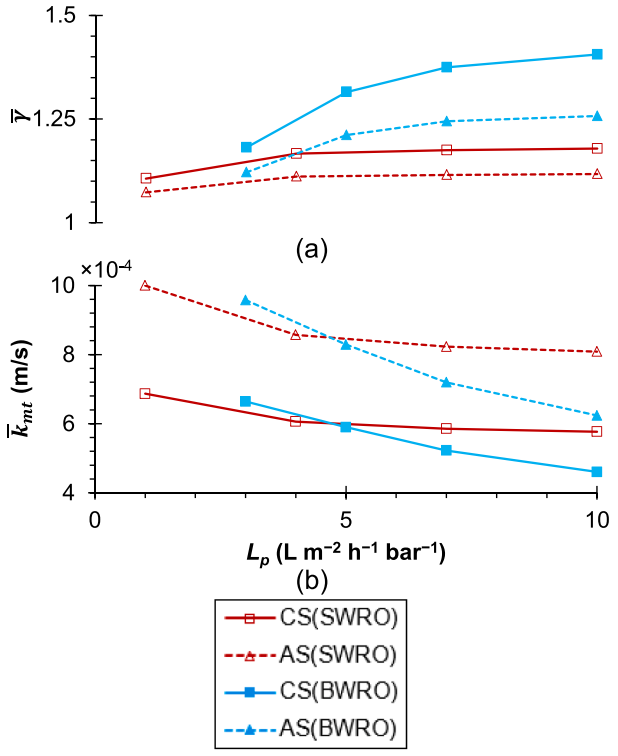

Fig. 4. Effect of intrinsic membrane permeance on (a) area-averaged concentration polarisation ($\overline{\gamma}$) and (b) mass transfer coefficient ($\overline{k}_{mt}$) at the same inlet TMP ($\Delta p_{tm,in,\ SW}$ = 6.5 MPa and $\Delta p_{tm,in,\ BW}$ = 1.5 MPa).

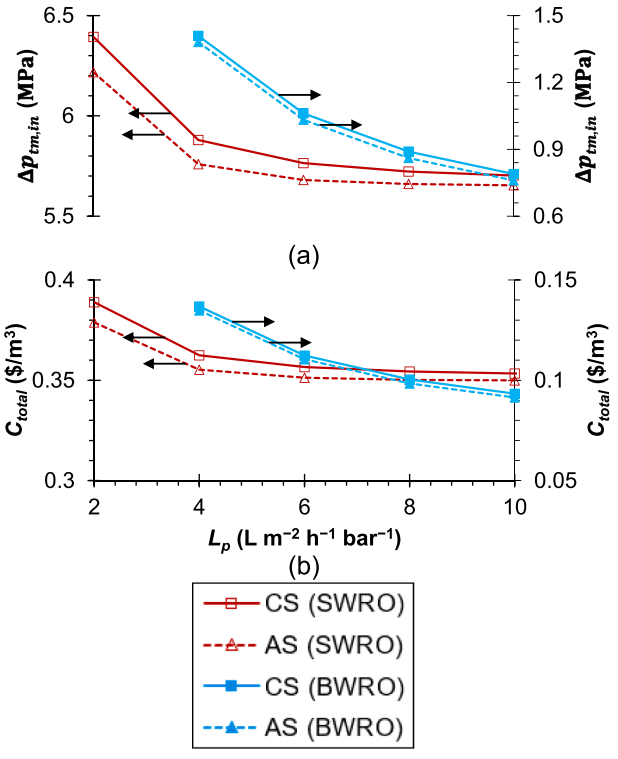

Fig. 5. Effect of intrinsic membrane permeance on (a) inlet transmembrane pressure ($\Delta p_{tm,in}$) and (b) total processing cost (C_{total}) at fixed R_r of 50% for SWRO and 70% for BWRO.

decreased water flux, even though those effects are not being considered in the calculation in this paper.

Fig. 5 shows the effect of membrane permeance on the corresponding total processing cost (C_{total}) when the membrane is operated at a fixed membrane length and recovery rate (50% for SWRO, and 70% for BWRO). As expected, the total processing cost decreases when permeance increases. This is because, at the same recovery, a higher membrane permeance requires a lower inlet pressure and hence lower energy cost (Fig. 5a). However, the rate of decrease in cost decreases as the permeance increases (Fig. 5b), and this is more evident for SWRO than for BWRO. As a consequence, the cost obtained when using the highest permeance membrane with a conventional spacer can be achieved at a lower permeance using an advanced spacer. This is particularly evident for SWRO, for which the total processing cost using the advanced spacer with a membrane permeance of 5 L m^{-2} h^{-1} bar^{-1} would require an almost doubling of the permeance (to about 10 L m^{-2} h^{-1} bar^{-1}) if using a conventional spacer. For BWRO, on the other hand, the advanced spacer shows less of an impact because relatively larger cost reductions are still possible by increasing membrane permeance. Nevertheless, the relevance of increasing membrane permeance (i.e., above 3 L m^{-2} h^{-1} bar^{-1}) is likely to remain in the near future, given that the current TFC RO membranes operate within the range of 1–3 L m^{-2} h^{-1} bar^{-1} [14–16]. Hence, there are still some prospects to reduce C_{total} by increasing membrane permeance, especially for BWRO. For SWRO, however, improving spacer performance is more likely to yield cost reductions than membrane permeance increases beyond 6 L m^{-2} h^{-1} bar^{-1}.

To ascertain whether the reported trends depend on the economic assumptions employed in this work, the sensitivity of the equivalent permeance ($L_{p,eq}$) to amortization factor, energy and membrane cost is analysed. The equivalent permeance is defined as the membrane permeance that, when using the advanced spacer, yields the same total cost as the highest permeance tested for the conventional spacer (10 L m^{-2} h^{-1} bar^{-1}). Fig. 6 shows that change in equivalent L_p is barely sensitive to the change in energy cost, and practically does not change despite large changes in amortization factor or membrane cost. Therefore, it is clear that the cost benefits of coupling advanced spacers to high-permeance membranes are independent of the economic assumptions.

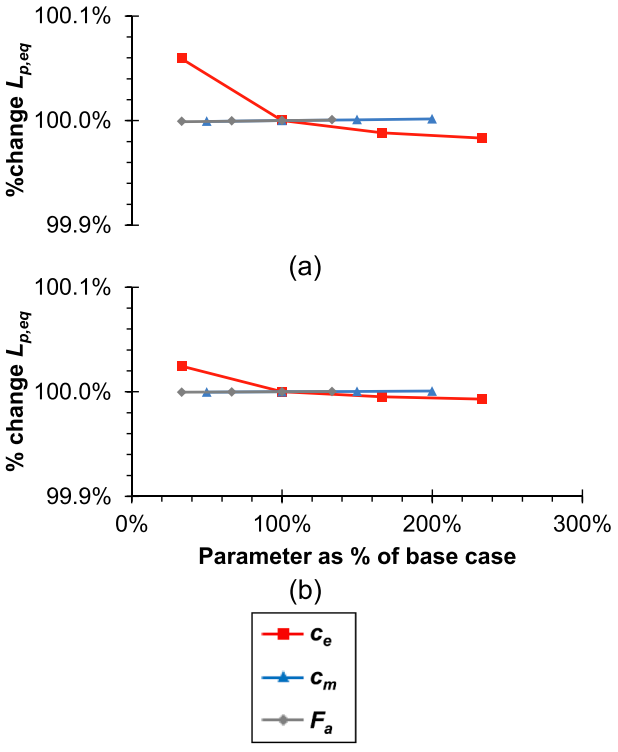

Fig. 6. Sensitivity analysis of the effect of amortization factor (F_a), energy (c_e) and membrane costs (c_m) on the percentage change in equivalent L_p when using the advanced spacer for (a) SWRO and (b) BWRO.

3.2. Effect of inlet transmembrane pressure ($\Delta p_{tm,in}$)

In general, C_{total} tends to increase with increasing $\Delta p_{tm,in}$ because of a larger driving force that requires higher energy consumption. However, this is not the trend for low-permeance BWRO (Fig. 7), where it can be seen that C_{total} decreases by 5% despite a 33% increase in the $\Delta p_{tm,in}$ when using a conventional spacer. This can be explained by the cost breakdown presented in Fig. 8, where it is shown that the operating pressure unit cost (C_{op}) remains almost constant despite increases in $\Delta p_{tm,in}$. This is because the rate of recovery increases faster than the cost due to the driving force, as $\Delta p_{tm,in}$ increases. Thus, C_{total} for low-permeance BWRO is mostly driven by the pre-treatment cost (C_{pt}), whereas a larger recovery increases the basis for the unit cost, thus decreasing C_{pt} and the overall total cost. It is worth noting that the decreasing trend in C_{total} is not applicable for low-permeance SWRO because the driving force required for SWRO is significantly larger than for BWRO (at least 4 times higher). Thus, C_{op} for SWRO is driven by the $\Delta p_{tm,in}$ rather than by the recovery rate.

3.3. Effect of feed conditions

This section investigates the feed flow conditions, i.e., feed concentration and velocity, on the total processing cost and recovery rate using a conventional spacer. As expected (see Fig. 9), an increase in feed concentration results in an increase of solute concentration near the membrane wall which in turn reduces flux and recovery rate, leading to an increase in C_{total} regardless of the value of membrane permeance at the same cross-flow velocity and driving force.

On the other hand, Fig. 10 presents the impact of inlet velocity on C_{total} and R_r for both the low and high-permeance membranes. It is interesting to note that C_{total} and R_r for high-permeance SWRO and BWRO remains basically unchanged within the range of feed velocity values typically encountered in RO operations. This is because, for a high-permeance membrane, the mass transfer coefficient ($k_{mt,per}$) and productivity of downstream module regions that were previously ineffective due to low flow rate and k_{mt} can be increased at a larger feed flow rate, as evidenced from Fig. 11. These results also show that the membrane flux approaches zero faster for the lower inlet velocity (i.e. 0.07 m/s, approaching zero flux at around 2 m from the inlet) than for the larger inlet velocity (i.e., 0.135 m/s, with near-zero flux after 3 m) for both high-permeance BWRO and SWRO.

4. Conclusion

The results of this techno-economic study show that, when operating at constant feed pressure, an advanced spacer that doubles mass transfer and reduces energy losses in a SWM module can only enhance flux more than the conventional spacer within the region close to the module inlet. This is because of the fast decrease in Reynolds number associated with a larger flux, which in turn results in a reduction in mass transfer downstream. Likewise, a high-permeance membrane also increases flux more toward the module inlet, which reduces the performance of the latter part of the module. This suggests that lower length modules in a tapered-array configuration might be the best configuration used for high-permeance membrane.

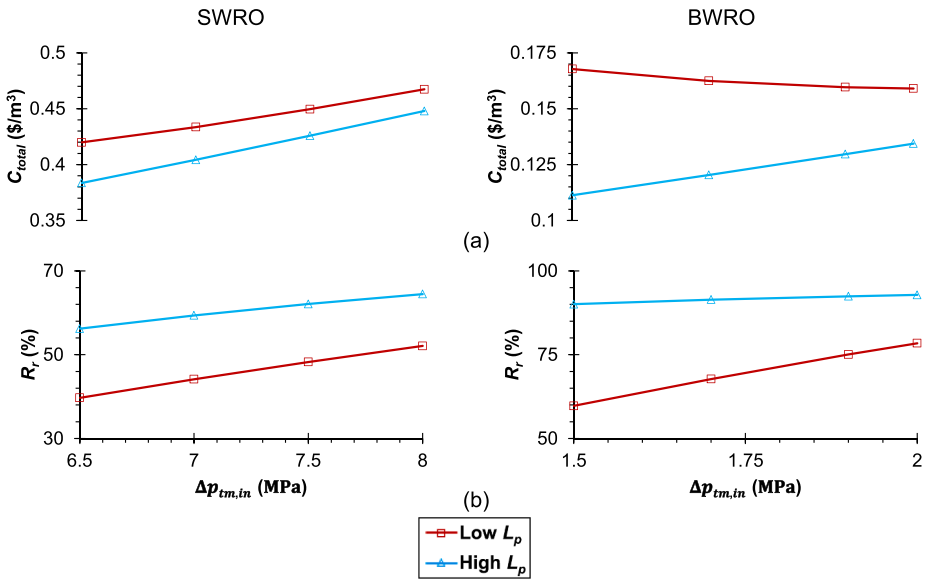

Fig. 7. Effect of $\Delta p_{tm,in}$ on (a) total processing cost (C_{total}) and (b) recovery rate (R_r) using conventional spacer for low ($L_{p,SW}$ = 1 L m^{-2} h^{-1} bar^{-1} and $L_{p,BW}$ = 3 L m^{-2} h^{-1} bar^{-1}) and high intrinsic membrane permeance ($L_{p,SW}$ = $L_{p,BW}$ = 10 L m^{-2} h^{-1} bar^{-1}), respectively.

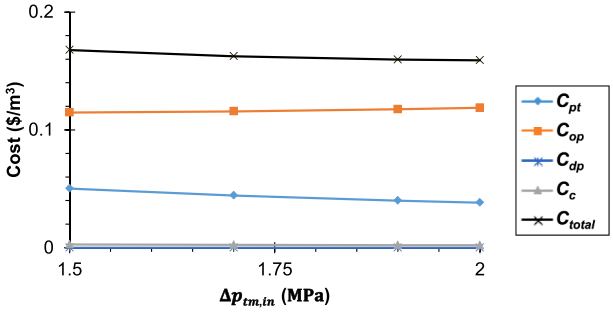

Fig. 8. Cost breakdown for low-permeance BWRO (using conventional spacer) as a function of $\Delta p_{tm,in}$.

This paper also found that when the membrane permeance is increased, the total processing cost can be reduced more for BWRO than for SWRO. Nevertheless, the effects are limited with further reductions in total processing cost when the membrane permeance exceeds 4 L m^{-2} h^{-1} bar^{-1} for SWRO and 7 L m^{-2} h^{-1} bar^{-1} for BWRO, owing to the high CP and lower mass transfer coefficient. This trend is similar to the SEC data reported in the literature [4,68] in which energy savings are negligible when L_p exceeds 4 and 5 L m^{-2} h^{-1} bar^{-1} for seawater and brackish water, respectively. Moreover, and despite not being included in the calculations presented in this paper, the tendency for fouling to occur (particularly scaling) is larger for high-permeance membranes, which could further reduce permeate flux and increase total processing costs if long modules are used.

When operating at constant recovery, it was shown that a higher membrane permeance requires less pumping energy. However, there

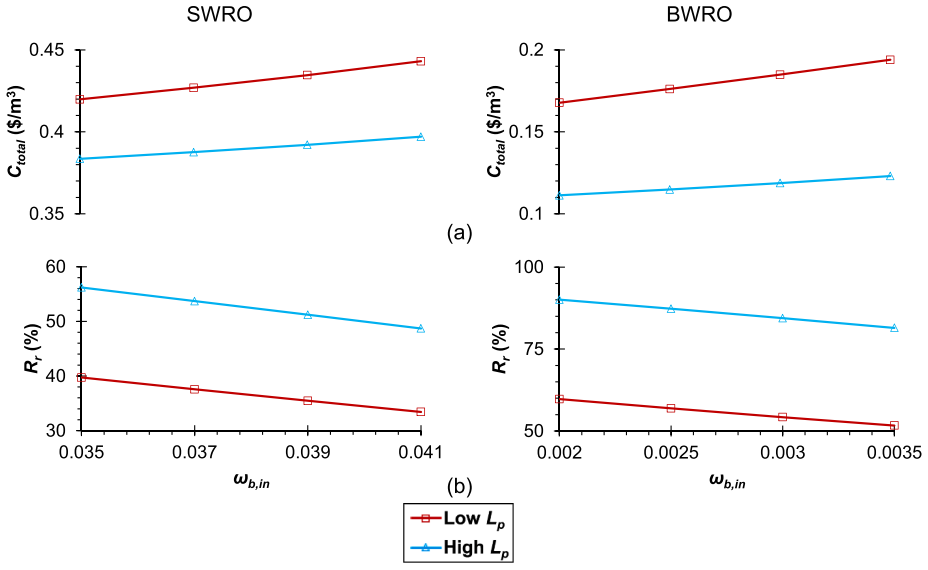

Fig. 9. Effect of feed concentration ($w_{b,in}$) on (a) total processing cost (C_{total}) and (b) recovery rate (R_r) using conventional spacer for low ($L_{p,SW}$ = 1 L m^{-2} h^{-1} bar^{-1} and $L_{p,BW}$ = 3 L m^{-2} h^{-1} bar^{-1}) and high intrinsic membrane permeance low ($L_{p,SW}$ = $L_{p,BW}$ = 10 L m^{-2} h^{-1} bar^{-1}), respectively.

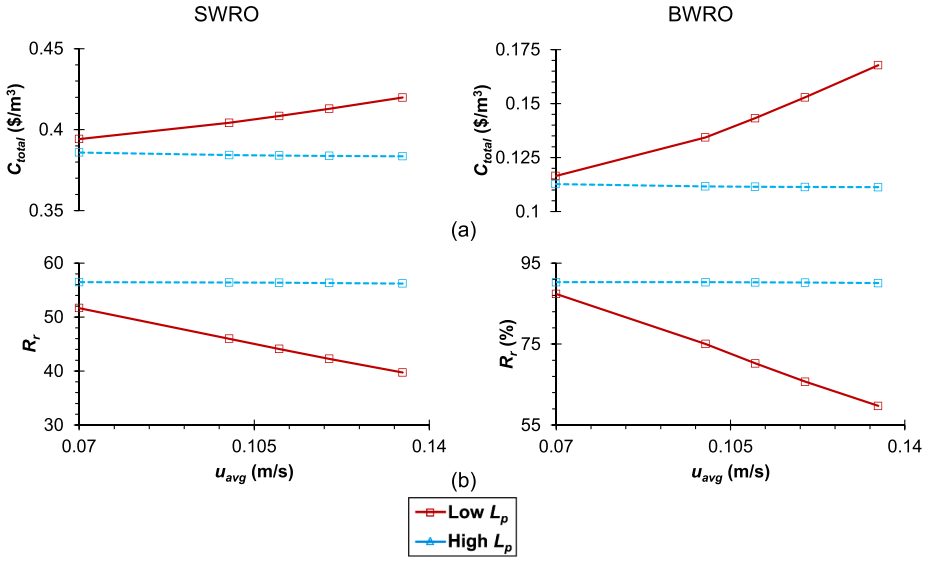

Fig. 10. Effect of inlet velocity (u_{avg}) on (a) total processing cost (C_{total}) and (b) recovery rate (R_r) using conventional spacer for low ($L_{p,SW}$ = 1 L m^{-2} h^{-1} bar^{-1} and $L_{p,BW}$ = 3 L m^{-2} h^{-1} bar^{-1}) and high intrinsic membrane permeance ($L_{p,SW}$ = $L_{p,BW}$ = 10 L m^{-2} h^{-1} bar^{-1}), respectively.

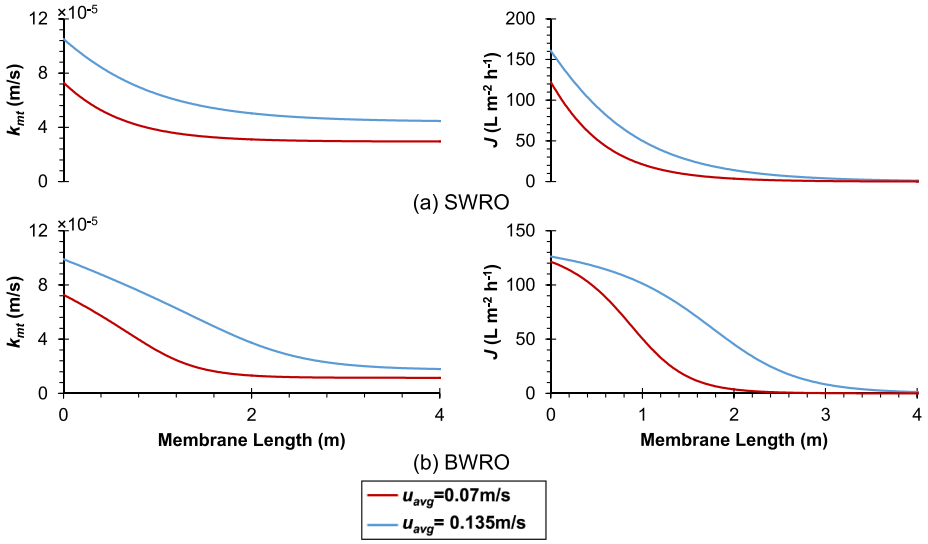

Fig. 11. Effect of inlet velocity (u_{avg}) on mass transfer coefficient ($k_{mt,per}$) for (a) SWRO and (b) BWRO under high intrinsic membrane permeance ($L_{p,SW}$ = $L_{p,BW}$ = 10 L m^{-2} h^{-1} bar^{-1}).

are diminishing returns in terms of cost reductions as the permeance increases. This means that an advanced spacer can achieve significant cost reductions at much lower permeance values than the conventional spacer, particularly for SWRO. For example, achieving the same total cost as the advanced spacer at a permeance of 5 L m^{-2} h^{-1} bar^{-1} required a near doubling of permeance if the conventional spacer was used. The use of an advanced spacer for BWRO, on the other hand, shows less potential because cost reductions are still possible as membrane permeance is increased. A sensitivity analysis revealed that the equivalent permeance ($L_{p,eq}$) is barely sensitive to the change in energy cost, and does not vary with changes in the amortization factor or membrane cost. Thus, the trends observed were practically independent of the economic assumptions made.

For low-permeance BWRO, the results reveal that the operating pressure unit cost is similar for any $\Delta p_{tm,in}$. This is because the associated $\Delta p_{tm,in}$ for BWRO is smaller compared to SWRO. Thus, the recovery rate increases at a faster rate than for an increase in cost due to a higher driving force. With respect to feed conditions, the results show that the total processing cost is similar for any feed velocity typically encountered for RO operations when using a high-permeance membrane. This is because, for a high-permeance membrane, the mass transfer coefficient or enhancement at a latter part of the module regions that were previously found ineffective due to low flow rate and k_{mt} can be enhanced at a larger feed velocity.

The main finding from this study is that when operating at constant recovery, improved spacer designs are more likely to yield cost reductions for SWRO than further increases in membrane permeance. These types of insights are gained through the use of the simplified techno-economic analysis method presented in this paper, which can be used to predict trends or relative changes in the magnitude of the total processing cost as the different operating and economic parameters are varied. However, this techno-economic methodology is restricted to steady-flow analysis, without any time-dependent fouling effects. Given that it is important to understand the effect of fouling on the flux and cost-effectiveness of SWM RO modules when membrane permeance or mass transfer is increased, future work is still required to shed further insights into these issues.

Nomenclature

Symbols

A_m	Membrane area in module (m^2)
C_c	Capital unit cost ($/$m^3$)
C_{dp}	Pressure drop unit cost($/$m^3$)
C_{op}	Operating pressure unit cost ($/$m^3$)
C_{pt}	Pre-treatment unit cost($/$m^3$)
C_{total}	Total processing unit cost ($/$m^3$)
c_e	Energy cost ($/kWh)
c_m	Membrane cost ($/$m^2$)
c_{total}	Total processing cost ($)
D	Solute diffusivity (m^2/s)
d_h	Hydraulic diameter (m)
F_a	Amortisation factor (yr^{-1})
f_{glob}	Fanning friction factor
h_{ch}	Channel height (m)
J	Permeate mass flux (kg m^{-2} s^{-1}, L m^{-2} h^{-1})
$k_{mt} = \frac{D}{w_w - w_b}\left(\frac{\partial w}{\partial y}\right)_w$	Mass transfer coefficient (m/s)
L	Membrane channel length (m)
L_p	Membrane permeance (L m^{-2} h^{-1} bar^{-1})
l_m	Mesh length (m)
N	Number of envelopes
p	Pressure (Pa)
Q	Volumetric flow rate (L/s, L/h)
$\Delta p_{tm,in}$	Inlet transmembrane pressure (Pa)
$R_{\text{int}} = 1 - \frac{w_p}{w_w}$	Membrane intrinsic rejection
R_r	Recovery rate
$\text{Re}_h = \frac{\rho \cdot u_{eff} \cdot d_h}{\mu}$	Hydraulic Reynolds number
$Sc = \frac{\mu}{\rho \cdot D}$	Schmidt number
$Sh = \frac{k_{mt} \cdot d_h}{D}$	Sherwood number
t_{op}	Operation time (h/yr)
u_{avg}	Inlet velocity (m/s)
$u_{eff} = \frac{u_{b,in}}{\varepsilon}$	Effective velocity (m/s)
w	Solute mass fraction
x	Distance in the bulk flow direction, parallel to membrane surface (m)
y	Distance from the bottom membrane surface, in direction normal to the surface (m)
z	Distance in the direction perpendicular to both x and y (m)

Greek letters

ε	Porosity
$\gamma = \frac{w_w - w_p}{w_b - w_p}$	Concentration polarisation modulus
μ	Dynamic viscosity (kg m^{-1} s^{-1})
η_{pump}	Pump efficiency
$\eta_R = \frac{p_0 - p_a}{(p_0 - p_a)_{ideal}}$	Retentate pressure recovery efficiency
π	Osmotic pressure (Pa)
$\pi_{in} = \varphi w_{b,\ in}$	Inlet osmotic pressure (Pa)
ρ	Fluid density (kg/m^3)
σ	Reflection coefficient
φ	Osmotic pressure coefficient (Pa)
ψ	Ratio of volumetric flux to impermeable mass transfer coefficient

Subscript

b	Value for the bulk flow
BW	Value for brackish water
f	Value for the feed
in	Value at the domain inlet
p	Value for the permeate
SW	Value for seawater
w	Value on the feed side membrane surface (wall)

CRediT authorship contribution statement

K.Y. Toh: Methodology, Validation, Formal analysis, Investigation, Writing - original draft.**Y.Y. Liang:**Conceptualization, Methodology, Validation, Formal analysis, Resources, Writing - review & editing, Supervision, Project administration, Funding acquisition.**W.J. Lau:**Writing - review & editing.**G.A. Fimbres Weihs:**Methodology, Formal analysis, Writing - review & editing.

Acknowledgements

The corresponding author would like to acknowledge the financial support provided by the Malaysia Ministry of Education under FRGS-RACER (Project number RDU192603). The first author (K.Y. Toh) gratefully acknowledges scholarship offered by Universiti Malaysia Pahang (UMP) throughout his study.

Appendix A. Flux calculation

In order to determine the permeate flux at each point of the SWM module, the CFD data for an impermeable dissolving wall case must first be converted to a permeable membrane case. The permeate mass flux (J) is determined based on the model of Kedem and Katchalsky [71]:

$$u_{y,w} = -\frac{J}{\rho} = -L_p(\Delta p_{tm} - \sigma\varphi R_{int} w_w) \tag{A1}$$

The mass balance on the membrane surface relates the permeate flux and mass fraction of solute at both sides of the membrane:

$$J\, w_w = \rho D\left(\frac{\partial w}{\partial y}\right)_w + J\, w_p \tag{A2}$$

The mass transfer coefficient can also be related with the interplay between the back-diffusion flux and its driving force, the mass fraction difference between the bulk and the membrane surface:

$$k_{mt} = \frac{D}{(w_w - w_b)}\left(\frac{\partial w}{\partial y}\right)_w \tag{A3}$$

Combining Eqs. (A1)–(A3) and the definition of intrinsic rejection (R_{int}) gives a quadratic equation for w_w that can be solved as follows:

$$w_w = w_p + \frac{1}{2\sigma\varphi}\left(\Delta p_{tm} - \frac{k_{mt}}{L_p}\right) + \sqrt{\left[\frac{1}{2\sigma\varphi}\left(\Delta p_{tm} - \frac{k_{mt}}{L_p}\right)\right]^2 + \frac{k_{mt}}{\sigma\varphi L_p}(w_b - w_p)} \tag{A4}$$

where w_p, σ, φ, Δp_{tm}, k_{mt}, L_p and w_b refer to permeate solute concentration, reflection coefficient ($\sigma = 1$), osmotic pressure coefficient ($\varphi = 8.051 \times 10^7$ Pa), transmembrane pressure ($\Delta p_{tm,in} = 6.50$ MPa for seawater; 1.50 MPa for brackish water), mass transfer coefficient for

permeable wall, membrane permeance and bulk solute concentration, respectively.

The Sh_{imp} obtained from impermeable wall correlations (Table 1) can be used for predicting the flux values for a permeable membrane ($k_{mt,per}$) using the correlation proposed by Geraldes & Afonso [50]:

$$\frac{Sh_{per}}{Sh_{imp}} = \frac{k_{mt,per}}{k_{mt,imp}} = \psi + (1 + 0.26\psi^{1.4})^{-1.7} \tag{A5}$$

where ψ is the ratio of volumetric flux to impermeable mass transfer coefficient:

$$\psi = \frac{J}{\rho k_{mt,imp}} \tag{A6}$$

For each point on the membrane surface, Eqs. (A1), (A4), (A5) and (A6) form a non-linear system that is solved iteratively, to find the permeable mass transfer coefficient ($k_{mt,per}$) and the permeate flux (J) under different operating conditions and membrane intrinsic properties (Table 2). It should be mentioned that the correlation in Eq. (A5) is only valid under conditions where $\psi < 20$ [50].

References

[1] J.M. Gordon, T.C. Hui, Thermodynamic perspective for the specific energy consumption of seawater desalination, Desalination 386 (2016) 13–18.
[2] D. Zarzo, D. Prats, Desalination and energy consumption. What can we expect in the near future? Desalination 427 (2018) 1–9.
[3] R. Semiat, Energy issues in desalination processes, Environmental Science & Technology 42 (2008) 8193–8201.
[4] D. Cohen-Tanugi, R. McGovern, S. Dave, J. Lienhard, J. Grossman, Quantifying the potential of ultra-permeable membranes for water desalination, Energy Environ. Sci. 7 (2014) 1134–1141.
[5] S.Y. Lim, Y.Y. Liang, G.A. Fimbres Weihs, D.E. Wiley, D.F. Fletcher, A CFD study on the effect of membrane permeance on permeate flux enhancement generated by unsteady slip velocity, J. Membr. Sci. 556 (2018) 138–145.
[6] Y. Okamoto, J.H. Lienhard, How RO membrane permeability and other performance factors affect process cost and energy use: a review, Desalination, 470 (2019) 114064.
[7] S. Mirza, Reduction of energy consumption in process plants using nanofiltration and reverse osmosis, Desalination 224 (2008) 132–142.
[8] T. Manth, M. Gabor, E. Oklejas, Minimizing RO energy consumption under variable conditions of operation, Desalination 157 (2003) 9–21.
[9] M. Qasim, M. Badrelzaman, N.N. Darwish, N.A. Darwish, N. Hilal, Reverse osmosis desalination: a state-of-the-art review, Desalination 459 (2019) 59–104.
[10] H.-J. Oh, T.-M. Hwang, S. Lee, A simplified simulation model of RO systems for seawater desalination, Desalination 238 (2009) 128–139.
[11] P.S. Goh, W.J. Lau, M.H.D. Othman, A.F. Ismail, Membrane fouling in desalination and its mitigation strategies, Desalination 425 (2018) 130–155.
[12] S.F. Anis, R. Hashaikeh, N. Hilal, Reverse osmosis pretreatment technologies and future trends: a comprehensive review, Desalination 452 (2019) 159–195.
[13] W.J. Lau, P. Goh, A. Ismail, S.-O. Lai, Ultrafiltration as a pretreatment for seawater desalination: a review, Membrane Water Treatment 5 (2014).
[14] C.Y. Chong, W.J. Lau, N. Yusof, G.S. Lai, N.H. Othman, T. Matsuura, A.F. Ismail, Studies on the properties of RO membranes for salt and boron removal: influence of thermal treatment methods and rinsing treatments, Desalination 428 (2018) 218–226.
[15] M. Chowdhury, J. Steffes, B. Huey, J. McCutcheon, 3D printed polyamide membranes for desalination, Science (New York, N.Y.) 361 (2018) 682–686.
[16] M. Elimelech, W. Phillip, The future of seawater desalination: energy, technology, and the environment, Science (New York, N.Y.) 333 (2011) 712–717.
[17] N. Misdan, W.J. Lau, A.F. Ismail, Seawater reverse osmosis (SWRO) desalination by thin-film composite membrane—current development, challenges and future prospects, Desalination 287 (2012) 228–237.
[18] W.-J. Lau, G.-S. Lai, J. Li, S. Gray, Y. Hu, N. Misdan, P.-S. Goh, T. Matsuura, I.W. Azelee, A.F. Ismail, Development of microporous substrates of polyamide thin film composite membranes for pressure-driven and osmotically-driven membrane processes: a review, J. Ind. Eng. Chem. 77 (2019) 25–59.
[19] N. Verma, S. Vaidh, G.S. Vishwakarma, A. Pandya, Chapter 18- antimicrobial nanomaterials for water disinfection, in: S. Rajendran, A. Mukherjee, T.A. Nguyen, C. Godugu, R.K. Shukla (Eds.), Nanotoxicity, Elsevier, 2020, pp. 365–383.
[20] Water Treatment Filter Made with the Proprietary Nanotechnology (TFN), in, LG Chem.
[21] Aquaporin Inside® Membranes, in, Aquaporin A/S.
[22] B. Shi, P. Marchetti, D. Peshev, S. Zhang, A.G. Livingston, Will ultra-high permeance membranes lead to ultra-efficient processes? Challenges for molecular separations in liquid systems, J. Membr. Sci. 525 (2017) 35–47.
[23] B. Mi, Graphene oxide membranes for ionic and molecular sieving, Science (New York, N.Y.) 343 (2014) 740–742.
[24] M. Hu, B. Mi, Enabling graphene oxide nanosheets as water separation membranes, Environmental Science & Technology 47 (2013).
[25] O. Kavianipour, G.D. Ingram, H.B. Vuthaluru, Investigation into the effectiveness of feed spacer configurations for reverse osmosis membrane modules using computational fluid dynamics, J. Membr. Sci. 526 (2017) 156–171.
[26] O. Kavianipour, G.D. Ingram, H.B. Vuthaluru, Studies into the mass transfer and energy consumption of commercial feed spacers for RO membrane modules using CFD: effectiveness of performance measures, Chem. Eng. Res. Des. 141 (2019) 328–338.
[27] H.S. Abid, D.J. Johnson, R. Hashaikeh, N. Hilal, A review of efforts to reduce membrane fouling by control of feed spacer characteristics, Desalination 420 (2017) 384–402.
[28] Y.Y. Liang, G.A. Fimbres Weihs, D.E. Wiley, Comparison of oscillating flow and slip velocity mass transfer enhancement in spacer-filled membrane channels: CFD analysis and validation, J. Membr. Sci. 593 (2020) 117433.
[29] C.P. Koutsou, A.J. Karabelas, A novel retentate spacer geometry for improved spiral wound membrane (SWM) module performance, J. Membr. Sci. 488 (2015) 129–142.
[30] B. Gu, C.S. Adjiman, X.Y. Xu, The effect of feed spacer geometry on membrane performance and concentration polarisation based on 3D CFD simulations, J. Membr. Sci. 527 (2017) 78–91.
[31] N. Sreedhar, N. Thomas, O. Al-Ketan, R. Rowshan, H. Hernandez, R.K. Abu Al-Rub, H.A. Arafat, 3D printed feed spacers based on triply periodic minimal surfaces for flux enhancement and biofouling mitigation in RO and UF, Desalination 425 (2018) 12–21.
[32] S. Kerdi, A. Qamar, J.S. Vrouwenvelder, N. Ghaffour, Fouling resilient perforated feed spacers for membrane filtration, Water Res. 140 (2018) 211–219.
[33] S.M. Ali, A. Qamar, S. Kerdi, S. Phuntsho, J.S. Vrouwenvelder, N. Ghaffour, H.K. Shon, Energy efficient 3D printed column type feed spacer for membrane filtration, Water Res. 164 (2019) 114961.
[34] G. Guillen, E.M.V. Hoek, Modeling the impacts of feed spacer geometry on reverse osmosis and nanofiltration processes, Chem. Eng. J. 149 (2009) 221–231.
[35] Z. Han, M. Terashima, B. Liu, H. Yasui, CFD investigation of the effect of the feed spacer on hydrodynamics in spiral wound membrane modules, Mathematical and Computational Applications 23 (2018) 17.
[36] N. Sreedhar, N. Thomas, O. Al-Ketan, R. Rowshan, H.H. Hernandez, R.K. Abu Al-Rub, H.A. Arafat, Mass transfer analysis of ultrafiltration using spacers based on triply periodic minimal surfaces: effects of spacer design, directionality and voidage, J. Membr. Sci. 561 (2018) 89–98.
[37] N. Thomas, N. Sreedhar, O. Al-Ketan, R. Rowshan, R.K. Abu Al-Rub, H. Arafat, 3D printed spacers based on TPMS architectures for scaling control in membrane distillation, J. Membr. Sci. 581 (2019) 38–49.
[38] N. Thomas, N. Sreedhar, O. Al-Ketan, R. Rowshan, R.K. Abu Al-Rub, H. Arafat, 3D printed triply periodic minimal surfaces as spacers for enhanced heat and mass transfer in membrane distillation, Desalination 443 (2018) 256–271.
[39] Y.Y. Liang, K.Y. Toh, G.A. Fimbres Weihs, 3D CFD study of the effect of multi-layer spacers on membrane performance under steady flow, J. Membr. Sci. 580 (2019) 256–267.
[40] A. Ruiz-García, I.N. Pestana, Feed spacer geometries and permeability coefficients. Effect on the performance in BWRO spriral-wound membrane modules, Water (Switzerland) 11 (2019).
[41] C.P. Koutsou, E. Kritikos, A.J. Karabelas, M. Kostoglou, Analysis of temperature effects on the specific energy consumption in reverse osmosis desalination processes, Desalination 476 (2020) 114213.
[42] A.J. Karabelas, C.P. Koutsou, M. Kostoglou, D.C. Sioutopoulos, Analysis of specific energy consumption in reverse osmosis desalination processes, Desalination 431 (2018) 15–21.
[43] F. Li, W. Meindersma, A.B. de Haan, T. Reith, Optimization of commercial net spacers in spiral wound membrane modules, J. Membr. Sci. 208 (2002) 289–302.
[44] A. Saeed, R. Vuthaluru, H.B. Vuthaluru, Investigations into the effects of mass transport and flow dynamics of spacer filled membrane modules using CFD, Chem. Eng. Res. Des. 93 (2015) 79–99.
[45] J. Schwinge, D.E. Wiley, D.F. Fletcher, Simulation of the flow around spacer filaments between channel walls. 2. Mass-transfer enhancement, Ind. Eng. Chem. Res. 41 (2002) 4879–4888.
[46] S.J. Im, S. Jeong, S. Jeong, A. Jang, Techno-economic evaluation of an element-scale forward osmosis-reverse osmosis hybrid process for seawater desalination, Desalination 476 (2020) 114240.
[47] M.A. Al-Obaidi, G. Filippini, F. Manenti, I.M. Mujtaba, Cost evaluation and optimisation of hybrid multi effect distillation and reverse osmosis system for seawater desalination, Desalination 456 (2019) 136–149.
[48] G. Filippini, M.A. Al-Obaidi, F. Manenti, I.M. Mujtaba, Design and economic evaluation of solar-powered hybrid multi effect and reverse osmosis system for seawater desalination, Desalination 465 (2019) 114–125.

[49] F. Li, W. Meindersma, A.B. de Haan, T. Reith, Novel spacers for mass transfer enhancement in membrane separations, J. Membr. Sci. 253 (2005) 1–12.
[50] V. Geraldes, M.D. Afonso, Generalized mass-transfer correction factor for nanofiltration and reverse osmosis, AICHE J. 52 (2006) 3353–3362.
[51] R.K. McGovern, J.H. Lienhard V, On the asymptotic flux of ultrapermeable seawater reverse osmosis membranes due to concentration polarisation, J. Membr. Sci. 520 (2016) 560–565.
[52] J.R. Werber, A. Deshmukh, M. Elimelech, The critical need for increased selectivity, not increased water permeability, for desalination membranes, Environmental Science & Technology Letters 3 (2016) 112–120.
[53] N.M. Mazlan, D. Peshev, A.G. Livingston, Energy consumption for desalination — a comparison of forward osmosis with reverse osmosis, and the potential for perfect membranes, Desalination 377 (2016) 138–151.
[54] Q. Wei, R. McGovern, J. V, Saving energy with an optimized two-stage reverse osmosis system, Environ. Sci.: Water Res. Technol. 3 (2017).
[55] G.A. Fimbres-Weihs, D.E. Wiley, Numerical study of two-dimensional multi-layer spacer designs for minimum drag and maximum mass transfer, J. Membr. Sci. 325 (2008) 809–822.
[56] S.A. Avlonitis, M. Pappas, K. Moutesidis, A unified model for the detailed investigation of membrane modules and RO plants performance, Desalination 203 (2007) 218–228.
[57] S.S. Bucs, R. Valladares Linares, J.O. Marston, A.I. Radu, J.S. Vrouwenvelder, C. Picioreanu, Experimental and numerical characterization of the water flow in spacer-filled channels of spiral-wound membranes, Water Res. 87 (2015) 299–310.
[58] DOW, DOW FILMTEC™ SW30-8040 Seawater Reverse Osmosis Element, in: T.D.C. Company (Ed.), Product Information, 2018.
[59] L.F. Greenlee, D.F. Lawler, B.D. Freeman, B. Marrot, P. Moulin, Reverse osmosis desalination: water sources, technology, and today's challenges, Water Res. 43 (2009) 2317–2348.
[60] W.N. Gill, D.E. Wiley, C.J.D. Fell, A.G. Fane, Effect of viscosity on concentration polarization in ultrafiltration, AICHE J. 34 (1988) 1563–1567.
[61] Y.Y. Liang, G. Fimbres Weihs, R. Setiawan, D. Wiley, CFD modelling of unsteady electro-osmotic permeate flux enhancement in membrane systems, Chem. Eng. Sci. 146 (2016) 189–198.
[62] Y.Y. Liang, G.A. Fimbres Weihs, D.F. Fletcher, CFD study of the effect of unsteady slip velocity waveform on shear stress in membrane systems, Chem. Eng. Sci. 192 (2018) 16–24.
[63] K. Mistry, J. Lienhard, Effect of Nonideal Solution Behavior on Desalination of a Sodium Chloride (NaCl) Solution and Comparison to Seawater, (2012).
[64] F. Elazhar, J. Touir, M. Elazhar, S. Belhamidi, N. El Harrak, A. Zdeg, M. Hafsi, Z. Amor, M. Taky, A. Elmidaoui, Techno-economic comparison of reverse osmosis and nanofiltration in desalination of a Moroccan brackish groundwater, Desalin. Water Treat. 55 (2015) 2471–2477.
[65] J.C. Quinn, R. Davis, The potentials and challenges of algae based biofuels: a review of the techno-economic, life cycle, and resource assessment modeling, Bioresour. Technol. 184 (2015) 444–452.
[66] A.H. Haidari, S.G.J. Heijman, W.G.J. van der Meer, Optimal design of spacers in reverse osmosis, Sep. Purif. Technol. 192 (2018) 441–456.
[67] H.A. Balogun, R. Sulaiman, S.S. Marzouk, A. Giwa, S.W. Hasan, 3D printing and surface imprinting technologies for water treatment: a review, Journal of Water Process Engineering 31 (2019) 100786.
[68] A. Shrivastava, S. Rosenberg, M. Peery, Energy efficiency breakdown of reverse osmosis and its implications on future innovation roadmap for desalination, Desalination 368 (2015) 181–192.
[69] T. Qiu, P. Davies, Comparison of configurations for high-recovery inland desalination systems, Water 4 (2012) 690.
[70] J. Schwinge, P.R. Neal, D.E. Wiley, D.F. Fletcher, A.G. Fane, Spiral wound modules and spacers: review and analysis, J. Membr. Sci. 242 (2004) 129–153.
[71] O. Kedem, A. Katchalsky, Thermodynamic analysis of the permeability of biological membranes to non-electrolytes, Biochim. Biophys. Acta 27 (1958) 229–246.